c-axis Josephson tunneling between $Bi_2Sr_2CaCu_2O_{8+x}$ and Pb

M. Mößle and R. Kleiner
Physikalisches Institut III, Universität Erlangen-Nürnberg, D-91058 Erlangen, Germany
(Received 28 August 1998)

We have fabricated Josephson tunnel junctions between $Bi_2Sr_2CaCu_2O_{8+x}$ (BSCCO) single crystals and Pb. Current flow is perpendicular to the CuO_2 double layers of the BSCCO single crystal. The surface of the crystals used is almost atomically flat with less than one half unit-cell growth step per 50 μm. At low temperatures, the current-voltage characteristics exhibit a well-developed Pb gap as well as a nonzero Josephson current. In external magnetic fields oriented parallel to the junction barrier the critical current follows closely a Fraunhofer diffraction pattern indicating that the critical current density is homogeneous over the whole junction area. In external microwave fields, Shapiro steps appear at voltages that are multiples of $f\Phi_0$ showing that the Josephson currents are caused by first-order tunneling processes. The results strongly indicate that the superconducting order parameter of BSCCO has a nonzero *s* component. The product of critical current I_c and normal-state resistance R_N of the junctions ranged between 0.5 and 8 μV, with an average value of 2.8 μV. An analysis of the I_cR_N products and of I_c vs temperature suggests that the *s* component is about three orders of magnitude smaller than the full order parameter that is generally presumed to have $d_{x^2-y^2}$ symmetry. [S0163-1829(99)01006-1]

I. INTRODUCTION

The exact symmetry of the superconducting order parameter in high-temperature superconductors is still the subject of ongoing debate.[1–7] Theories based on a repulsive pairing interaction predict pure $d_{x^2-y^2}$ symmetry, and, at least for some high-temperature superconductors, there is convincing experimental evidence that the order parameter has indeed $d_{x^2-y^2}$ symmetry. Most experiments have been done on $YBa_2Cu_3O_7$ (YBCO),[8–27] $Bi_2Sr_2CaCu_2O_{8+x}$ (BSCCO),[28–34] and $Tl_2Ba_2CuO_6$ (TBCO).[31–36] On the other hand, *c*-axis tunneling experiments between YBCO and Pb have shown that there must be a nonvanishing *s* component of the superconducting order parameter in YBCO.[37–45] The amount of *s* relative to $d_{x^2-y^2}$, however, is unclear. Most *c*-axis experiments are basically insensitive even to a huge $d_{x^2-y^2}$ component. On the other hand, phase-sensitive experiments probing the sign change of the $d_{x^2-y^2}$ component in the CuO_2 planes can allow for a relatively large admixture of *s* before the sign change is lost. From the small values of the product of the critical current I_c and the normal-state resistance R_N, as measured in the *c*-axis experiments, one might guess that the *s* part is small, possibly on the order of a few per cent or less. A (small) *s* component of the order parameter of YBCO may have simple explanations. YBCO has an orthorhombic distortion occurring along the Cu-O bonds of the CuO_2 layers. As a result, the $d_{x^2-y^2}$ order parameter and the *s* order parameter belong to the same representation of the crystal symmetry group. Admixtures $d\pm s$ may lead to a distorted order parameter as shown in Fig. 1. In addition, the CuO chains located between the CuO_2 layers might be superconducting as well, making the situation even more complicated. In order to decide whether or not a *s* component is inherent to high-temperature superconductivity there is thus a strong need to extend investigations to more simple materials. There are hints from torque measurements that TBCO has mixed $d+s$ symmetry.[46] The critical current of BSCCO Josephson junctions formed between CuO_2 layers being twisted with respect to each other about the *c* axis shows basically no dependence on the twist angle.[47,48,6]

It was our intention to investigate *c*-axis tunnel junctions between Pb and BSCCO in analogy to the *c*-axis Pb/YBCO experiments. There are no CuO chains in BSCCO, but there is a distortion of the CuO_2 layers due to a superstructure in the BiO layers. However, the distortion of the CuO_2 layers is diagonal to the Cu-O bonds[49,50] and should lead at most to a diagonally distorted *d*-wave order parameter (cf. Fig. 1). As a result, the *s* and $d_{x^2-y^2}$ order parameters belong to different representations of the crystal symmetry group and should not mix.[51] In that case, positive and negative contributions from the (distorted) *d*-wave order parameter to the *c*-axis supercurrent completely cancel each other. Thus a nonzero supercurrent in a *c*-axis Pb/BSCCO Josephson tunnel junction cannot be explained by trivial reasons.

Experiments with *c*-axis Pb/BSCCO junctions have recently been performed by several groups; in these experi-

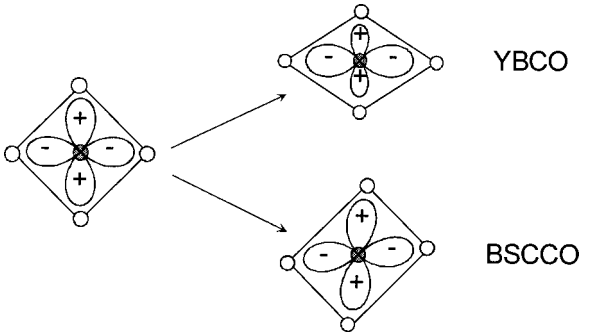

FIG. 1. Schematic drawing of order-parameter distortion in YBCO and BSCCO, respectively. Rectangles symbolize the CuO_2 layer, and the open and gray circles symbolize O and Cu, respectively.

ments no Josephson current was observed.[52,53] In Ref. 54 we reported results where the Josephson current was nonzero. At that stage the homogeneity of the critical current density of the samples was far from perfect. For the results presented in this paper, we improved our preparation technique. In our experiments, we evaporate Pb electrodes onto the surface of freshly cleaved BSCCO single crystals. BSCCO cleaves easily between the BiO layers, and, as a result, almost atomically flat surfaces can be produced. In order to show that BSCCO has an *s*-wave order-parameter component, we proceed as follows. We measure current-voltage (*I*-*V*) characteristics at various temperatures, in external magnetic fields directed parallel to the CuO_2 layers of the crystal, and in external microwave fields. From the shape of the *I*-*V* characteristics, information on the quality of the tunneling barrier can be obtained. For a good tunnel junction, the subgap resistance should be as large as possible and a well-developed Pb gap should be present. In addition, there should be fine structures 4 and 8 mV above the Pb gap associated with the electron-phonon coupling in Pb, assuring that the tunneling process is single stage.[55] In the presence of a Josephson current, its homogeneity can be measured by recording the magnetic-field dependence of the critical current. In principle, a nonzero Josephson current can result from second-order tunneling processes even for a pure $d_{x^2-y^2}$ order parameter.[56] Such processes can be identified or ruled out by measuring microwave-induced steps in the *I*-*V* characteristics.[43] If the Josephson current is uniform and of first order, it has to arise from an *s*-wave component of the order parameter in BSCCO. More quantitative conclusions about the magnitude and the critical temperature of this component can subsequently be drawn from an analysis of the I_cR_N products and the temperature dependence of the critical current. In this paper we will show that our junctions fulfill almost all quality criteria. The only quantity we were not able to determine was the Pb phonon structure. Due to intrinsic Josephson junctions[57–70] located underneath the Pb/BSCCO junctions it was impossible to obtain sufficiently large voltages across the Pb/BSCCO junction. We will show that an *s* component of the order parameter is present; its magnitude is most likely three orders of magnitude smaller than the *d* component.

II. EXPERIMENT

The BSCCO crystals were grown in oxygen atmosphere out of a stoichiometric mixture of the oxides and carbonates.[71] X-ray diffraction confirmed that the crystals were single phase Bi(2212), and electron-induced x-ray analysis indicated a cation stoichiometry of approximately Bi:Sr:Ca:Cu 2.3:2.2:1:2. In order to achieve a homogeneous oxygen content the crystals were annealed in oxygen for 8–10 h at 420 °C. The inductively measured critical temperature of the crystals was 87 K, with a transition width of 2 K. For the experiments single crystals of typically $1\times3\times0.1$ mm^3 were selected. They were embedded in epoxy with only one surface parallel to the CuO_2 planes uncovered. Immediately before evaporation of the Pb counter electrode the uppermost BSCCO layers were removed with a sticky tape in order to get a very clean and smooth surface. After this step the edges and a part of the outermost surface of the crystal were covered by epoxy leaving a window of approximately 0.2×1.5 mm^2 of free BSCCO surface. The samples were then mounted into a vacuum chamber and three, typically 0.3 mm wide, stripes of Pb, plus interlayers, were evaporated through a shadow mask. With this procedure, three *c*-axis Pb/BSCCO tunnel junctions are formed with two sides of each junction defined by the Pb stripes, and the other two sides defined by the edge of the epoxy layer. We fabricated junctions with pure Pb electrodes, with Pb/In and Pb/Bi alloys, as well as with Au or Ag interlayers between Pb and BSCCO. The thicknesses of the interlayers were varied between 1 and 6 nm. Without interlayer, tunnel junctions exhibiting a well-developed Pb gap and a nonzero supercurrent could be made; however, these junctions degraded within a few minutes due to a strong oxygen reduction of the uppermost BSCCO layers by the Pb electrode. For these samples, the resistance of the tunnel barrier was about 1 $m\Omega\,cm^2$, and the critical supercurrent density was about 1 mA/cm^2. With interlayers the time scale for degradation increased to 1–2 h, and the barrier resistance dropped to values between 0.5 $\mu\Omega\,cm^2$ and 1 $m\Omega\,cm^2$. Correspondingly, the critical supercurrent densities increased to values between 4 mA/cm^2 and 5.5 A/cm^2. The best and most reproducible results were obtained for a 1-μm-thick Pb layer and a 2-nm-thick Ag interlayer. Unless otherwise stated, measurements presented in this paper were made with junctions fabricated with this procedure.

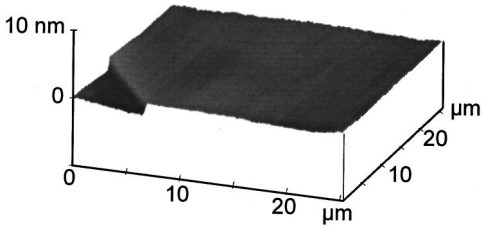

FIG. 2. AFM picture of a 25×25 μm^2 section of the surface of a cleaved BSCCO single crystal showing one growth step of 15 Å height.

For a well-defined *c*-axis tunnel contact the BSCCO surface should be as plane as possible. Growth steps might produce a contact in *ab* direction, and the measured supercurrents might trivially result from tunneling along the planes. However, the fact that BSCCO cleaves easily along the BiO layers allowed us to produce extremely flat surfaces. We measured the surface roughness of three samples by atomic force microscopy (AFM). Altogether 30 pictures were made. Most pictures showed one growth step with a height of one-half unit cell of the BSCCO crystal in an area of 30×30 μm^2. Seven pictures were even free of any step. Figure 2 shows a typical example. In the figure one growth step with 15 Å height (a half unit cell) can clearly be seen. From the AFM data we calculated the ratio between the area in *ab* direction and the area in *c* direction to 2×10^{-5}. If the supercurrent were to flow exclusively through the sidewalls of the growth steps, the critical supercurrent densities would have to be as large as some 10^5 A/cm^2, a value that already would be exceptionally large for tunnel junctions. Also, within a typical junction length of 0.3 mm there are only about five growth steps. We will show later that the magnetic-field dependence of the critical supercurrent fol-

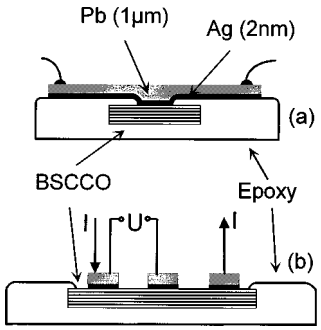

FIG. 3. Schematic drawing of the *c*-axis Pb/BSCCO junctions. (a) shows the BSCCO crystal embedded in epoxy with the 1-μm-thick Pb and the 2-nm-thick Ag layer; (b) shows the arrangement of the electrical contacts to the three junctions. In the configuration shown in (b) the *I-V* characteristic of the left junction is measured.

lows an almost perfect Fraunhofer pattern; this cannot be explained by current flow exclusively through the sidewalls of the growth steps.

One voltage and one current lead were connected to each Pb electrode with conductive silver paste. Any of the three junctions could be measured in a four-terminal configuration by using one of the remaining junctions as current lead and the other as voltage lead. Figure 3 shows a schematic drawing of the junction geometry with the three Pb electrodes on a BSCCO single crystal embedded in epoxy. In Fig. 3(a) one 1-μm -thick Pb electrode and the 2-nm-thick Ag interlayer are shown. Figure 3(b) shows the setup for the measurement of the *I-V* characteristics. Current flow is from the left to the right electrode through the uppermost layers of the BSCCO crystal. The voltage is measured between the left and the middle Pb electrode. In this case the left Pb/BSCCO junction is measured. For the measurements the samples were mounted in vacuum. All measurements were done in triple μ-metal shielding and in an electrically shielded environment. Temperatures could be varied between 1.7 K and 300 K. Microwave fields from 2 to 20 GHz were applied via a semiridgid cable. Magnetic fields of up to 10 G directed parallel to the CuO_2 layers and parallel to the long sides of the Pb stripes were applied by a superconducting coil. In order to avoid trapped flux, the samples had to be cooled as slow as 0.2 K/min through T_c of BSCCO. These slow cooling rates in a shielded environment were essential for measuring Josephson supercurrents.

III. RESULTS AND DISCUSSION

In this section will first focus on *I-V* characteristics at low temperatures. Then we will address the temperature dependence of the *I-V* characteristics and the critical current. In the third part, measurements in magnetic fields are discussed. Finally, we will present data measured in external microwave fields.

A. *I-V* characteristics at low temperatures

Figures 4(a) and 4(b) show the *I-V* characteristic of sample mb232 as measured at $T=1.8$ K on two different current and voltage scales. There is a Josephson current with

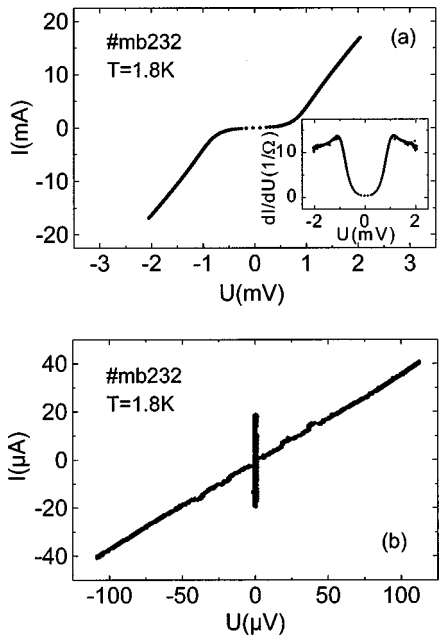

FIG. 4. *I-V* characteristic of sample mb232 at $T=1.8$ K (a) on large current and voltage scales and (b) on expanded current and voltage scales. Inset in (a) shows differential conductance dI/dU vs U.

a critical current of $I_c=20$ μA [Fig. 4(b)]. The junction area was 0.04 mm^2 yielding a critical current density $j_c=32$ mA/cm^2. The *I-V* characteristic is highly hysteretic with a return current $I_r=1.6$ μA. For voltages below 100 μV the (subgap) resistance is approximately linear, $R_s \approx 2.8$ Ω. With increasing voltage the differential resistance decreases reaching a minimum of 0.072 Ω at a voltage of about 1.3 mV. At larger voltages the *I-V* characteristic becomes linear with a differential resistance of $R_N=0.074$ Ω ($R_N A=30$ $\mu\Omega\,cm^2$), a factor of 38 less than R_S. The ratio R_s/R_N is on the lower side of what could be expected for a tunnel junction at low temperatures. However, we will show later in Fig. 7(c), that R_s has not yet saturated at 1.8 K. Thus, R_s/R_N can be expected to increase further at lower temperatures. The voltage position of the resistance minimum is close to the ideal value of the Pb gap, 1.35 mV, showing that the order parameter on the Pb side essentially keeps its full value at the barrier. It also shows that no or at least no significant (minimum) energy gap is present on the BSCCO side. This is certainly the case if the order parameter of BSCCO had pure $d_{x^2-y^2}$ symmetry. In the presence of a (small) *s* component the order parameter would still be gapless if the admixture occurs in the form $s \pm d$. For an admixture $s \pm id$ the *s* component would lead to a nonzero energy gap. However, we will show in the next section that Δ_s is most likely less than 20 μV for an admixture $s \pm id$. This value is too small to shift the resistance minimum measurably from the Pb gap value. Since the *I-V* characteristic is almost linear at low voltages [Fig. 4(b)], the resistively shunted junction (RSJ) model[72,73] with R_s as the resistor may be used to analyze the hysteresis of the *I-V* characteristic and to extract the junction capacitance and the dielectric constant of the barrier. Within the RSJ model, the ratio I_r/I_c is determined by the McCumber parameter $\beta_c=2\pi I_c R_s^2 C/\Phi_0$. Here, C denotes the junction capacitance and Φ_0 is the flux

TABLE I. Parameters of some of the Pb/BSCCO junctions. All samples listed here were prepared with a 1-μm-thick Pb layer as electrode and Ag as interlayer. The interlayer thickness d is listed in the last column.

Sample	A (mm^2)	I_c (μA)	R_N (Ω)	I_cR_N (μV)	R_NA ($\mu\Omega\,cm^2$)	j_c (A/cm^2)	d (nm)
mb232	0.040	20	0.074	1.5	29.6	0.05	2
mb172	0.049	1000	0.005	5	2.54	2.04	2
mb173	0.033	850	0.009	7.7	2.97	2.60	2
mb162	0.088	160	0.043	6.9	37.8	0.18	2
mb122	0.052	190	0.04	7.6	20.8	0.375	1.5
mb123	0.062	28	0.043	1.2	26.7	0.045	1.5
mb103	0.06	6	0.27	1.6	162	0.01	2.5
mb023	0.06	3280	0.0008	2.6	0.48	5.47	6
pb253	0.48	100	0.03	3	144	0.021	6
pb231	0.011	1	0.5	0.5	55	0.0091	6
pb223	0.053	5	1	5	530	0.0094	6

quantum. For $\beta_c \gg 1$, $I_r/I_c \approx 4/\pi\sqrt{\beta_c}$. The measured value $I_r/I_c \approx 0.08$ corresponds to a β_c of about 250. By using the measured values $I_c = 20$ μA and $R_s = 2.8\,\Omega$ one finds $C = 1.6$ nF. With an estimated barrier thickness of 1 nm this yields a reasonable value for the dielectric constant of about 4.5. The product of critical current and normal resistance of sample mb232 at 1.8 K is 1.5 μV. Note that this value is much less than what could be expected for the I_cR_N product between two *s*-wave superconductors. Using the expression (valid at $T = 0$ K) (Ref. 75)

$$I_cR_N = \frac{2\Delta_{\mathrm{Pb}}\Delta_{\mathrm{BSCCO}}}{\Delta_{\mathrm{Pb}}+\Delta_{\mathrm{BSCCO}}} K\left(\frac{\Delta_{\mathrm{BSCCO}}-\Delta_{\mathrm{Pb}}}{\Delta_{\mathrm{BSCCO}}+\Delta_{\mathrm{Pb}}}\right), \qquad (1)$$

where K denotes the complete elliptic integral, and a value Δ_{BSCCO} of 25–30 mV,[76] one would estimate $I_cR_N \approx 6$ mV, which is three orders in magnitude larger than the measured values of 0.5–8 μV. However, I_cR_N values of some μV are comparable to values measured for *c*-axis Pb/YBCO tunnel junctions on YBCO thin films.[40] For temperatures below 10 K R_N was essentially temperature independent. For sample mb232, for example, R_N was 0.07 Ω at $T = 8$ K, just above T_c of the Pb electrode, in good agreement with the value measured below T_c. For that reason, we routinely determined R_N at 8 K for all samples.

We have measured *I-V* characteristics of about 50 samples, where we used different materials for the electrodes and the interlayers. All junctions showed a substantial supercurrent and a clear Pb energy gap. The best results were obtained for the 25 junctions made with pure Pb as electrode and Ag as interlayer. Junctions made with other materials, for example, Pb-Bi or Pb-In as electrodes and Au as interlayer, were not as homogeneous as the Pb/Ag/BSCCO junctions. Table I contains properties for a selection of junctions out of the Pb/Ag/BSCCO series. Junction areas could be varied between 0.01 and 0.5 mm^2. The Josephson current densities j_c ranged between 4 mA/cm^2 and 5.5 A/cm^2, R_NA between 0.5 $\mu\Omega\,cm^2$ and 800 $\mu\Omega\,cm^2$. The variation for a given thickness of the Ag layer is stronger than any systematic variation with the Ag thickness. Most likely, the reason for the strong varation in j_c and R_N is the variation in the time elapsed between deposition of the Pb electrodes and cooldown. Despite the j_c and R_N variation by up to three orders of magnitude, the I_cR_N product was always between 0.5 μV and 8 μV, with an average value of 2.8 μV. The weak variation of I_cR_N can be seen more clearly in Fig. 5 where we show $I_cR_N(T = 1.8$ K) vs I_c for all samples out of the Pb/Ag/BSCCO series.

For sample mb232 (Fig. 4) the *I-V* characteristic was only measurable for bias currents up to 20 mA, where the voltage across the junction was about 2 mV. For larger currents, Ohmic heating warmed up the crystal. Nonetheless some samples could be traced up to higher voltages. An example is shown in Fig. 6(a) for sample mb122, measured at $T = 2$ K, where the maximum voltage was 8 mV. This sample had a critical current of 190 μA [lower right inset in Fig. 6(a)]. For bias currents above 13.6 mA the *I-V* characteristic develops an additional branch. Figure 6(b) shows an *I-V* characteristic of the same sample measured at $T = 8$ K. The critical current of the Pb/BSCCO junction as well as the Pb gap have disappeared [cf. inset in Fig. 6(b)], whereas the additional jump still occurs at essentially the same current. Also note that for currents below the jump the *I-V* curve is linear. There is no indication of a zero bias anomaly that should be expected if part of the current were to flow parallel to the CuO_2 layers.[53] This further confirms that the current transport is perpendicular to the layers.

Multiple branching is well known from *c*-axis transport measurements of BSCCO single crystals.[57–70] It starts when the weakest intrinsic Josephson junction, formed by adjacent CuO_2 double layers, switches into the resistive state. In direct measurements of the intrinsic Josephson effect stacks of

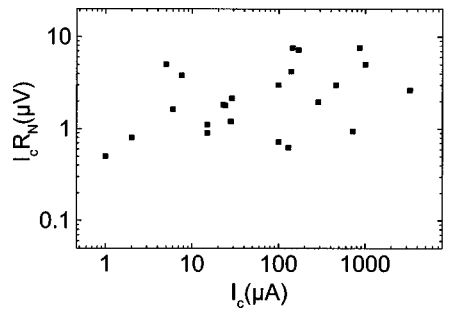

FIG. 5. Product of critical current and normal resistance I_cR_N vs critical current I_c. I_c was measured at 1.8 K, and R_N was determined at 8 K.

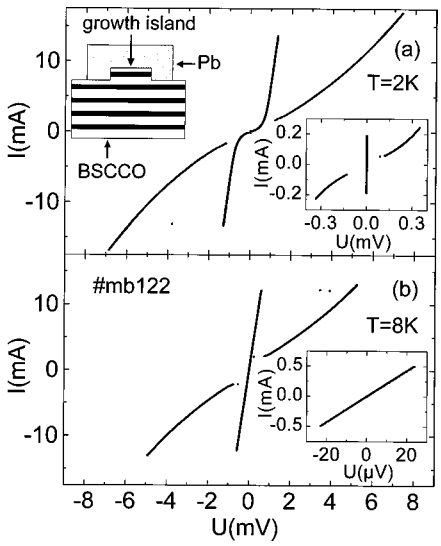

FIG. 6. *I-V* characteristic of sample mb122 at a temperature of (a) 2 K and (b) 8 K showing an additional branch due to an intrinsic junction switching to the resistive state. Lower right inset in (a) and inset in (b) show the *I-V* characteristic on expanded current and voltage scales. Upper left inset in (a) shows a schematic drawing of the proposed location of the intrinsic junction.

intrinsic Josephson junctions are usually made by patterning mesa structures on top of BSCCO single crystals. In the geometry discussed here, no mesa structure is—at least on purpose—fabricated underneath the Pb/BSCCO junction. However, the Ag and Pb layers cover some growth islands (cf. Sec. II) such that ''mesas'' formed by these islands are connected in series with the Pb/BSCCO junction [cf. upper left inset in Fig. 6(a)]. For (artificially patterned) mesa structures, the characteristic voltage of intrinsic junctions, i.e., the voltage jump at the critical current of a given junction, is typically 25 mV.[77] In contrast, in the geometry discussed here we often find much smaller values. For example, the voltage jump in Fig. 6(a) is 5 mV. However, reduced values of V_c are not surprising since the growth steps are at least partially covered—and thus shunted—by the Ag and Pb layer. An example where V_c is close to optimum is discussed in Schlenga *et al.*[77] We have seen the additional branching in many samples. Often, some 3–5 additional branches appeared. Typically, the branching occurred at currents 2–3 orders of magnitude larger than I_c.

In the context of tunneling between Pb and BSCCO the appearance of the additional branches is important at least in two ways. First, they prevent measuring the pure *I-V* characteristic of the Pb/BSCCO junction up to large voltages. For example, the maximum voltage drop across the Pb/BSCCO junction in Fig. 6(a) was 1.3 mV. Measurements beyond 4 mV would be important to detect Pb phonon structures (located 4 and 8 mV above the Pb gap.[55]) So far, none of the samples allowed the measurement of these structures. Second, however, the additional branches can be used as sensors to probe the critical temperature of the CuO_2 layers located next to the Pb/BSCCO interface simply by measuring the critical current of the intrinsic junctions (and its disappearance) as a function of temperature. For the sample shown in Fig. 6, T_c was 36 K and for the other samples T_c varied between 28 and 60 K (cf. Table II). In contrast, the bulk

TABLE II. Critical current, characteristic voltage, and critical temperature of the weakest intrinsic Josephson junction for five Pb/BSCCO samples.

Sample	$I_{c,\text{intrinsic}}$ (mA)	V_c (mV)	T_c (K)
mb122	13.6	5.0	36
mb123	0.6	17	60
mb103	16	4.8	55
mb232	16	2.9	28
pb231	0.5	0.1	50

critical temperature of the BSCCO single crystals was around 87 K. It seems natural to ascribe the reduced T_c of the outermost layer to a strong oxygen reduction by the Pb film. As a consequence, all measurements discussed here were performed on strongly underdoped BSCCO.

B. Temperature dependence

We now return to the properties of the Pb/BSCCO junction and discuss *I-V* characteristics as function of temperature. In Fig. 6 we already showed that the Josephson current disappeared above the critical temperature of the Pb electrode. The temperature dependence of the *I-V* characteristic of sample mb232 below 8 K is more clearly shown in Fig. 7 for $T=3.1$ K, 5.5 K and 8 K. Note that a measurement of

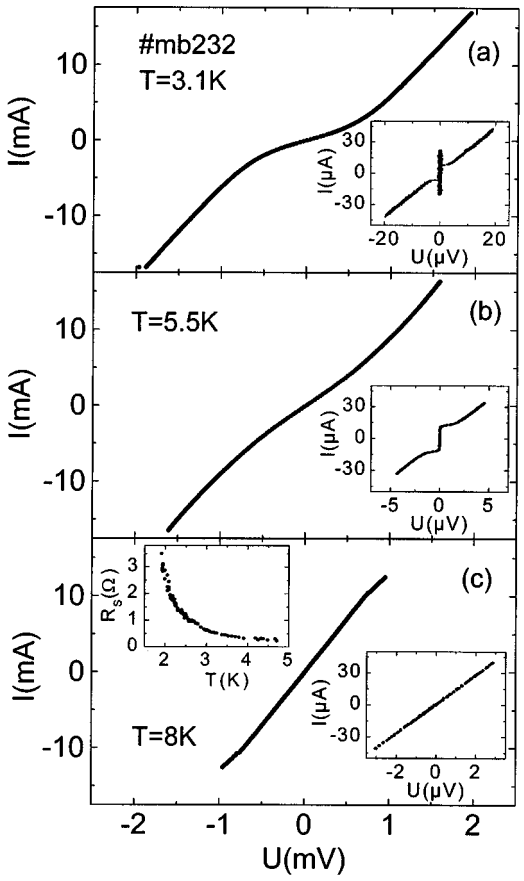

FIG. 7. *I-V* characteristics of sample mb232 at (a) 3.1 K, (b) 4.2 K, and (c) 8 K. Insets in (a), (b), and lower right inset in (c) show the same characteristic on expanded current and voltage scales. Upper left inset in (c) shows R_s vs temperature.

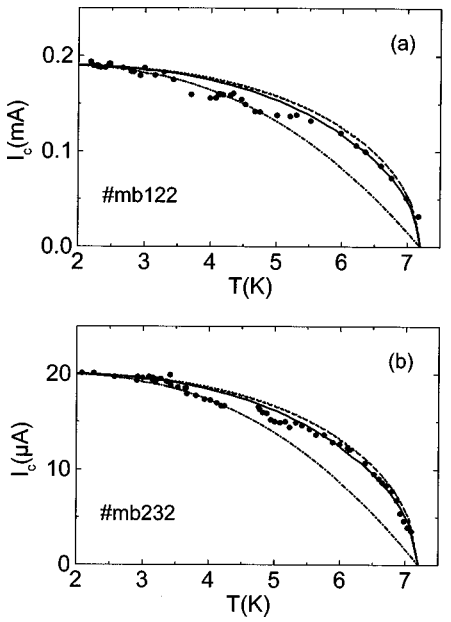

FIG. 8. Critical current of samples mb122 (a) and mb232 (b) vs temperature (markers). Dotted lines in (a) and (b) correspond to a BCS temperature dependence of the energy gap with $T_c = T_{c,Pb} = 7.2$ K. Curves in (a) correspond to Eq. (2) in the $s \pm id$ case with $T_{c,d} = 36$ K, $\Delta_d = 30$ meV, $\Delta_s = 18.5$ μeV and $T_{c,s} = 12$ K (solid line), $T_{c,s} = 36$ K (dashed line), and $T_{c,s} = 7.2$ K (dash-dotted line). Curves in (b) correspond to Eq. (2) with $T_{c,d} = 28$ K, $\Delta_d = 30$ meV, $\Delta_s = 3.65$ μeV and $T_{c,s} = 11$ K (solid line), $T_{c,s} = 36$ K (dashed line), and $T_{c,s} = 7.2$ K (dash-dotted line).

the same sample at $T = 1.8$ K is shown in Fig. 4. When the temperature is increased from 1.8 K, the subgap resistance strongly decreases. For example, its value at 3.1 K is 0.55 Ω [Fig 7(a)], and its value at 5.5 K is 0.13 Ω [Fig. 7(b)]. The dependence of R_s on temperature is shown as an upper left inset in Fig. 7(c). Note, that down to the lowest measurement temperature, 1.8 K, no saturation is observable. As a result of the decrease of R_s with increasing temperature, the I-V characteristic becomes nonhysteretic around 5.5 K. Thus, $\beta_c \approx 1$. Using the capacitance $C = 1.6$ nF as calculated above, and with $R_s = 0.13$ Ω, $I_c = 12$ μA at $T = 5.5$ K, we calculate $\beta_c \approx 0.98$ in very good agreement.

Figures 8(a) and 8(b) show the critical current of samples mb122 and mb232 as a function of temperature. At $T = 2$ K, the samples have $I_c R_N$ products of 7.6 μV and 1.5 μV, respectively. In order to extract information from $I_c(T)$ we adopt Tanaka's and Kashiwaya's theory for tunneling between s-wave and d-wave superconductors.[78] We assume that the Pb order parameter has pure s symmetry, whereas the order parameter on the BSCCO side has both an s and a d component. As discussed by Klemm *et al.*,[51] for the crystal symmetry of BSCCO an admixture s and $d_{x^2-y^2}$ would have to be of the form $s \pm i d_{x^2-y^2}$. However, for the sake of completeness, we will also discuss admixtures $s \pm d$. We then may write $\Delta_{\mathrm{BSCCO}} = \Delta_s \pm \Delta_d \cos 2\phi$, or $\Delta_{\mathrm{BSCCO}} = \Delta_s \pm i\Delta_d \cos 2\phi$.[79] We numerically calculate the expression

$$I_c(T) = \frac{k_B T}{2eR_N} \sum_{n=0,\pm 1,\pm 2,\ldots} \int_0^{2\pi} d\phi \times \frac{\Delta_{\mathrm{Pb}}(T)\Delta_{\mathrm{BSCCO}}(T)}{\sqrt{\omega_n^2 + \Delta_{\mathrm{Pb}}^2(T)}\sqrt{\omega_n^2 + |\Delta_{\mathrm{BSCCO}}(T)|^2}} \qquad (2)$$

with the Matsubara frequencies $\omega_n^2 = 2\pi k_B T(n + \frac{1}{2})$. Equation (2) has been derived under the assumptions that the Fermi surface (of BSCCO) is nearly two dimensional and that the supercurrent arises from first-order tunneling. First-order tunneling between a pure s-wave superconductor and a pure d-wave superconductor does not lead to a nonzero Josephson current and, as a consequence, Eq. (2) yields $I_c R_N = 0$ for $\Delta_s = 0$. For evaluation of Eq. (2) we assume a BCS temperature dependence of Δ_{Pb}, Δ_s, and Δ_d.[80] For sample mb122, the critical temperature of the outermost BSCCO layer, as determined from the disappearence of the critical current of the weakest intrinsic junction, was 36 K. Thus it seems natural to fix at least the critical temperature of the d component $T_{c,d}$ to $T = 36$ K. In order to compare Eq. (2) with the measured value of I_c we assume that R_N does not depend on temperature. We first discuss the $s \pm id$ case. The dashed line in Fig. 8(a) is for $\Delta_d = 30$ meV and $\Delta_s = 18.5$ μeV. For these parameters, Eq. (2) yields $I_c R_N(T = 2\ \mathrm{K}) = 7.6$ μV, as measured for sample mb122. The calculated $I_c(T)$ follows closely the temperature dependence of Δ_{Pb}, which is shown as dotted line in Fig. 8(a). Near T_c, the calculated $I_c(T)$ is slightly steeper than the measured $I_c(T)$. We next varied Δ_d between 10 meV and 30 meV while keeping $T_{c,d}$ as well as the critical temperature of the s component $T_{c,s}$ fixed to 36 K. Within this range, an $I_c R_N$ value of 7.6 μV at 2 K was achieved for Δ_s between 9.5 and 18.5 μeV, i.e., for a ratio Δ_d/Δ_s between 1000 and 2000. In all cases, the calculated $I_c(T)$ followed very closely the temperature dependence of Δ_{Pb}. An s component might not necessarily have the same T_c as the d component. Therefore, in a second step we also varied $T_{c,s}$ for $T_{c,d} = 36$ K and $\Delta_d = 30$ meV. As minimum value we tested $T_{c,s} = T_{c,\mathrm{Pb}}$. Best agreement with the measured $I_c(T)$ is achieved for $T_{c,s} = 12$ K [solid line in Fig. 8(a)]. For $T_{c,s} < 11$ K, $I_c(T)$ was well below the measured curve and did not fit the data. As an example, we show the curve with $T_{c,s} = T_{c,\mathrm{Pb}}$ as dash-dotted line in Fig. 8(a). Curves for $T_{c,s}$ between 12 K and 36 K were between the dashed and the solid curve in Fig. 8(a). For all values of $T_{c,s}$ an $I_c R_N(2\ \mathrm{K})$ of 7.6 μV was achieved for about the same value of $\Delta_s \approx 18.5$ μV. For an admixture $s \pm d$ a somewhat larger value of Δ_s, 51.5 μV, is required to reproduce the measured $I_c R_N$ product. With the altered Δ_s, the curves for a given value of $T_{c,s}$ are almost indistinguishable from the $s \pm id$ case. Best agreement with the data would be for $T_{c,s} = 11$ K.

For sample mb232 [Fig. 8(b)] the critical temperature of the weakest intrinsic junction was 28 K. Thus $T_{c,d}$ was fixed to 28 K and $T_{c,s}$ was varied between 7.2 and 28 K. We obtained the best fit to the measured data for $T_{c,s} = 11$ K, $\Delta_d = 30$ meV, and $\Delta_s = 3.65$ μeV (solid line). For these parameters Eq. (2) yields $I_c R_N(T = 2\ \mathrm{K}) = 1.5$ μV as measured. For comparison, we again show the temperature dependence of Δ_{Pb} as dotted line, and the cal-

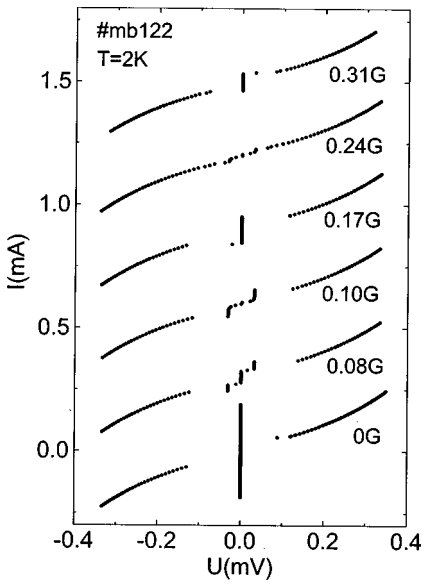

FIG. 9. *I-V* characteristic of sample mb122 for six values of magnetic field applied parallel to the BSCCO layers, measured at 2 K. For clarity, curves are vertically offset. The modulation of the critical current with magnetic field as well as the appearance of a Fiske step is clearly seen.

culated $I_c(T)$ for $T_{c,s}=T_{c,d}=28$ K, $\Delta_d=30$ meV, $\Delta_s=3.65$ μeV (dashed line), and for $T_{c,s}=T_{c,\mathrm{Pb}}$, $T_{c,d}=28$ K, $\Delta_d=30$ meV, $\Delta_s=3.65$ μeV (dash-dotted line). For this sample, an admixture $s\pm d$ would require $\Delta_s=10.2$ μV and $T_{c,s}=10$ K for the best fit.

Δ_d might be as large as 50 mV;[81] in that case, for an admixture $s\pm id$ ($s\pm d$), Δ_s would increase to 26 μeV (79 μeV) for sample mb122, and to 5.1 μeV (15.5 μeV) for sample mb232. In any case a value of Δ_s below 80 μeV seems to be sufficient to fit the data. This would mean that the fraction of the *s* component relative to the *d* component is less than some 10^{-3}. There is indication that $T_{c,s}$ is smaller than $T_{c,d}$ or, alternatively, that Δ_s depends stronger on temperature than expected from a BCS temperature dependence of Δ. (Note that, at $T=7.2$ K, for a $T_{c,s}$ of 12 K, Δ_s has decreased to 90% of its zero temperature value, whereas for a $\Delta_{c,s}$ of 36 K $\Delta_s(7\ \mathrm{K})/\Delta_s(0\ \mathrm{K})=0.9999$). However, the difference between $T_{c,s}=12$ K and $T_{c,s}=36$ K is small and thus the evidence for a reduced $T_{c,s}$ is at most weak. More important is the fact that $T_{c,s}=T_{c,\mathrm{Pb}}$ is not consistent with the data. If the *s* component were induced by proximity we would expect $T_{c,s}$ close to $T_{c,\mathrm{Pb}}$. $I_c(T)$ thus strongly indicates that the *s* component does not simply arise from proximity to Pb.

C. Magnetic-field dependence

We begin this section with a discussion of the *I-V* characteristics of the Pb/BSCCO junctions measured in magnetic fields applied parallel to the CuO_2 planes of the BSCCO crystal. Figure 9 shows *I-V* characteristics of sample mb122 at $T=2$ K for six values of the magnetic field. For clarity, curves are vertically offset. At zero field, $I_c=190$ μA. For $B=0.08$ G, I_c decreased to 25 μA and a step appears at a voltage $U=32$ μV. For $B=0.1$ G, the supercurrent is almost zero, and the height of the step at 32 μV reaches its maximum value of 43 μA. Curves for $B=0.17$ G, 0.24 G and 0.31 G show subsequent maxima and minima of I_c. The step at 32 μV can be identified as a Fiske resonance.[82,74] Fiske steps should appear at multiples of voltages $U=\Phi_0\bar{c}/2b$; b is the junction width perpendicular to the magnetic field, and $\bar{c}=c\sqrt{d/\varepsilon t_{\mathrm{eff}}}$ is the Swihart velocity. Here, $d\approx 1$ nm denotes the barrier thickness and $t_{\mathrm{eff}}=(\lambda_{\mathrm{BSCCO}}+\lambda_{\mathrm{Pb}}+d)$ is the effective-field penetration depth; $\lambda_{\mathrm{BSCCO}}\approx 170$ nm and $\lambda_{\mathrm{Pb}}\approx 47$ nm are the field penetration depths into the BSCCO and Pb electrodes, respectively. From this expression, with $U=32$ μV, $b=300$ μm, one finds $\bar{c}=9\times 10^6$ m/s, and $\varepsilon\approx 5$ in good agreement with the estimate of Sec. III A.

We now turn to the magnetic-field dependence of the critical current $I_c(B)$. For a homogeneous junction with lateral dimensions not much larger than the Josephson penetration depth $\lambda_J=\sqrt{\Phi_0/(2\pi\mu_0 j_c t_{\mathrm{eff}})}$, $I_c(B)$ is described by the Fraunhofer pattern $I_c(B)/I_c(0)=|\sin x/x|$, with $x=\pi A_{\mathrm{eff}}B/\Phi_0$ and $A_{\mathrm{eff}}=t_{\mathrm{eff}}b$. For the samples discussed below, λ_J ranged between 200 μm and 600 μm, and b was between 100 μm and 400 μm. Thus, b is on the order of λ_J and the junctions can be considered as short junctions. A junction width of 400 μm yields $A_{\mathrm{eff}}=87.2$ μm^2, and the zeros of the critical current should occur at multiples of $B_0=0.24$ G. For $b=200$ μm, $B_0=0.48$ G. For many junctions the measured magnetic-field dependence of I_c was close to the Fraunhofer diffraction pattern. Three examples are shown in Fig. 10. For sample mb173 [Fig. 10(a)] the zeros of I_c occur at multiples of 0.34 G. For this sample, $b=230$ μm; the effective area is thus about a factor 1.5 larger than expected, possibly due to either flux compression into the barrier or to a somewhat larger value of λ_{BSCCO}, which should be expected for underdoped BSCCO. The solid line in Fig. 10(a) corresponds to $|\sin x/x|$. Data are very close to this curve showing that the junction is homogeneous. Data could only be measured to slighty more than 1 G. For larger fields (Josephson) flux quanta penetrated in between the CuO_2 layers of the BSCCO crystal leading to a hysteretic behavior of $I_c(B)$. Figure 10(b) shows $I_c(B)$ for sample mb162 with a width of 260 μm. Data are again very close to the Fraunhofer diffraction pattern, with the zeros of I_c occurring at multiples of 0.24 G, a factor of 1.5 below the expected value. Figure 10(c) shows $I_c(B)$ for sample mb122. The first zero of I_c occurs at 0.1 G, but the next zeros are not exact multiples of B_0. The solid line in the figure shows $I_c(B)$ as calculated for the spatially varying critical current density shown in the inset. The current density peaks at the edges; however, it is still not too far from homogeneous. In particular, critical current densities as homogeneous as measured cannot arise from supercurrents flowing through the sidewalls of growth steps.

D. Microwave irradiation

In the above sections we have implicitly assumed that the *c*-axis supercurrent between BSCCO and Pb arises from first-order tunneling processes. As shown by Tanaka,[56] higher-order tunneling processes lead to a nonvanishing Josephson

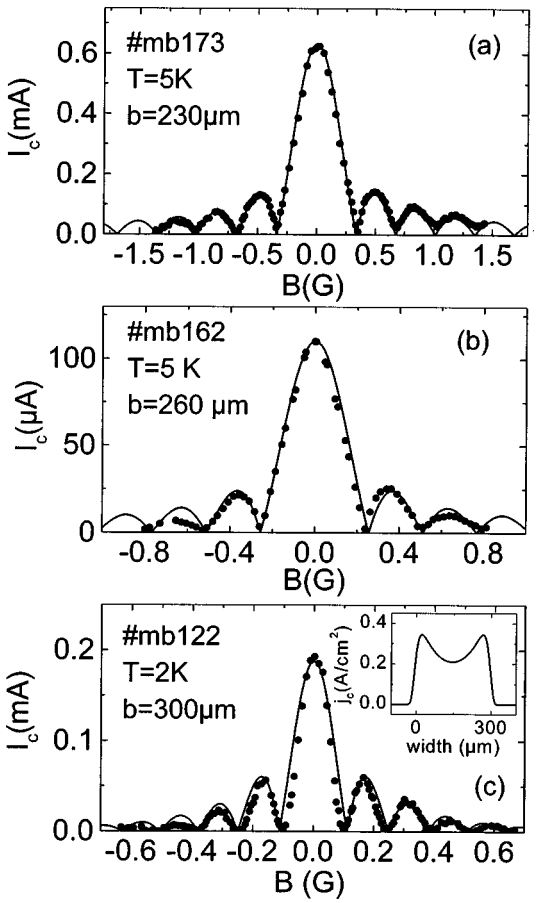

FIG. 10. Magnetic-field dependence of the critical current for samples (a) mb173, (b) mb162, and (c) mb122. Solid lines in (a) and (b) correspond to Fraunhofer pattern $I_c(B)/I_c(0)=|\sin x/x|$, with $x=\pi A_{\rm eff}B/\Phi_0$. Solid line in (c) is calculated $I_c(B)$ using the critical current density distribution shown in the inset.

current even in the absence of an *s*-wave component of the order parameter. In that case, the Josephson current phase relation becomes π periodic ($I=I_c\sin 2\delta$). For conventional Josephson tunnel junctions, such second-order processes do not contribute much to the total supercurrent because of the small tunneling probability. However, since the measured values of I_cR_N are extremely small, the supercurrent could in principle be caused by second-order processes. Second-order contributions can be identified easily by measuring *I-V* characteristics in external microwave fields. For conventional Josephson tunnel junctions microwave-induced steps appear at multiples of $U=f\Phi_0$. Here, f is the frequency of the external microwave field. In the limit of $\beta_c\gg 1$, and with f larger than the Josephson plasma frequency $f_{\rm pl}=\sqrt{I_c/C\Phi_0}$, the amplitude of the step at $U_n=nf\Phi_0$, with $n=0,\pm 1,\pm 2,\ldots$ is given by the nth Bessel function $I_n=I_c|J_n(U_{\rm ac}/f\Phi_0)|$.[74] Here, $U_{\rm ac}$ is a rf drive amplitude. For our junctions, $f_{\rm pl}\approx 1$ GHz. In contrast, the π-periodic current phase relation in the case of pure second-order tunneling leads to microwave-induced steps at voltages $U_n=\frac{1}{2}n\Phi_0$; their amplitudes are given by $I_n=I_c|J_n(2U_{\rm ac}/f\Phi_0)|$. In the case of *c*-axis Pb/YBCO junctions, experiments in external microwave fields have proven that the Josephson current observed in these junctions is due to first-order tunneling, with upper limits for second-order contributions of about 1%.[43] In the

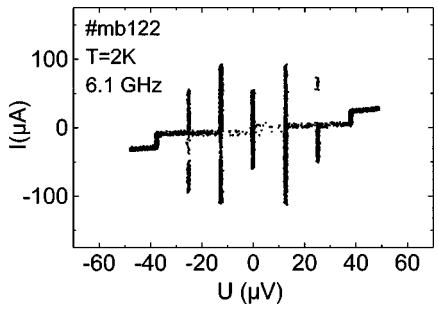

FIG. 11. *I-V* characteristic of sample mb122 at 2 K in a 6.1-GHz microwave field.

experiments discussed here, microwaves were applied in a range from 2 to 20 GHz for various temperatures. Figure 11 shows the *I-V* characteristic of sample mb122 in a 6.1 GHz microwave field at $T=2$ K. Microwave-induced steps occur at voltages $U=nf\Phi_0$, but not at voltages $U=(n+\frac{1}{2})f\Phi_0$. The steps overlap strongly and even cross the voltage axis. Since the junction was current biased, only some of the possible Shapiro steps could be traced out during one cycle. After many cycles, however, random switching ensured that all steps were included, even if their amplidude was much smaller than that of their neighbors. The *I-V* characteristics shown in this section were recorded with a storage oscilloscope, and all points that have been recorded through many cycles are shown. From Fig. 11 it is already evident that the observed supercurrent is at least dominantly of first order and, consequently, that an *s* component of the order parameter must be present. In order to get more quantitative results we first look at the Shapiro step amplitudes as a function of $U_{\rm ac}$. In the presence of both a first- and a second-order contribution, the total supercurrent may be written as $I=I_0[(1-\alpha)\sin\delta_o+\alpha\sin(2\delta_0+\phi)]$;[43] $\alpha=0$ corresponds to purely first-order tunneling, and $\alpha=1$ to purely second-order tunneling. The phase shift ϕ may be 0 or π, corresponding to an admixture $s\pm d$, or $\pi/2$ or $3\pi/2$, corresponding to an admixture $s\pm id$. In that case, the amplitude of the Shapiro step at $U=nf\Phi_0$ is given by

$$I_n=I_0\ \max[(1-\alpha)J_n(U_{ac}/f\Phi_0)\sin\delta_0 + \alpha J_{2n}(2U_{ac}/f\Phi_0)\sin(2\delta_0+\phi)], \quad (3)$$

where one has to maximize I_n with respect to δ_0. The results are shown in Fig. 12(a) to 12(c) for $\alpha=0$ (solid lines), and for $\alpha=0.1$ for the cases $s\pm d$ (dotted lines) and $s\pm id$ (dashed lines). The curves differ only weakly, and the data, taken from sample mb162 at $f=7.2$ GHz and from sample mb023 at $f=4.8$ GHz, clearly cannot distinguish between $\alpha=0$ and $\alpha=0.1$. However, the fact that the data are very well described by the Bessel function allows one to find the microwave drive level where a possible step at $U=\frac{1}{2}f\Phi_0$ would be largest. A more stringent limit for α can be set by closely investigating the *I-V* characteristic at this value of U_{ac}. The height of this step is given by

$$I_{1/2}=\alpha I_0|J_1(2U_{ac}/f\Phi_0)|. \quad (4)$$

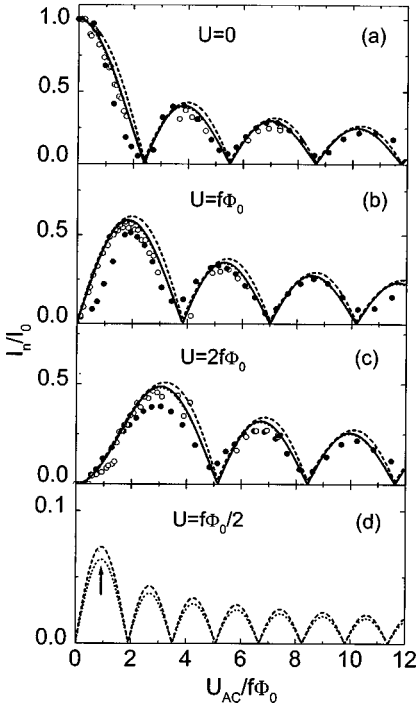

FIG. 12. Measured step amplitudes at $U=0$ (a), $U=f\Phi_0$ (b), and $U=2f\Phi_0$ (c) for samples mb162 (open symbols) and mb023 (solid symbols) at microwave frequencies of 7.2 GHz (mb162) and 4.8 GHz (mb023). Solid lines in (a) to (c) are computed step amplitudes for first-order tunneling ($\alpha=0$), dotted lines are for $s\pm d$ with $\alpha=0.1$, and dashed lines are for $s\pm id$ with $\alpha=0.1$. Data are fitted to the first maximum of J_0. (d) Amplitude of steps at $U=\frac{1}{2}f\Phi_0$, with the same notation and $\alpha=0.1$. The arrow indicates the value of $U_{ac}/f\Phi_0$ at which these steps have their maximum.

Figure 12(d) shows $I_{1/2}$ for $\alpha=0.1$ for the cases $s\pm d$ (dotted lines) and $s\pm id$ (dashed lines). $I_{1/2}$ is largest when I_0 has decreased to about 77% of its value for $U_{\rm ac}=0$. Here, $I_1/I_0\approx\frac{1}{2}$, and I_2 is almost zero. Figure 13 shows the I-V characteristics for two samples (mb122 and 162), irradiated with the appropriate microwave power. Figures 13(a) and 13(b) are for sample mb122 on different current scales, and Figs. 13(c) and 13(d) for sample mb162 on different current scales. Both samples as well as all other measured samples showed no steps at $U=\frac{1}{2}f\Phi_0$. For sample mb122, we would have been able to detect a step with an amplitude of 3 μA, and for sample mb162 the minimum detectable step height was 4.3 μA. With these values, from an analysis of Eqs. (3) and (4) we then extract upper limits of $\alpha=3\%$ (mb122) and $\alpha=4.5\%$ (mb162). Values for some other samples are listed in Table III. The data clearly show that any second-order distribution to the supercurrent would have to be less than a few per cent. What would we expect for α assuming that the ratio Δ_d/Δ_s were 10^4? Basically, α is given by Δ_d/Δ_s times the tunneling probability p; we do not know the exact p; reasonable numbers might range between 10^{-6} and 10^{-10}. For the largest value, we would expect an $\alpha\approx1\%$, which is just below our resolution. On the other hand, for $p=10^{-10}$, α could be as small as 10^{-6}; in that case, second-order contributions would clearly be undetectable.

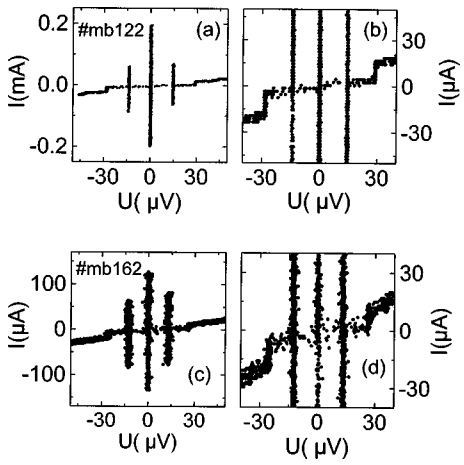

FIG. 13. I-V characteristics at a microwave amplitude close to the value where the step at $U=\frac{1}{2}f\Phi_0$ is predicted to be maximum; (a) and (b) are I-V characteristics of sample mb122 at 2 K in a 6.9-GHz microwave field on different current scales, and (c) and (d) are I-V characteristics of mb162 on different current scales ($T=2$ K, $f=6.4$ GHz).

TABLE III. Upper boundary α of second-order contributions to supercurrent for a selection of samples.

Sample	$\alpha[s+d]$ (%)	$\alpha[s+id]$ (%)
mb232	3.5	3.0
mb173	3.5	3.0
mb172	2.5	2.0
mb162	4.5	4.0
mb122	3.0	2.5
pb253	2.0	1.5
pb223	2.0	1.5

IV. CONCLUSIONS

We successfully prepared c-axis Pb/BSCCO high-quality Josephson tunnel junctions. All junctions exhibited a nonzero supercurrent. The critical current follows closely the Fraunhofer diffraction pattern showing that the critical current density is essentially homogeneous. Together with the fact that the surfaces of our BSCCO single crystals are almost atomically flat it can be ruled out that the supercurrent arises exclusively from shunts through sidewalls of residual growth steps. We have clear evidence from microwave experiments that the Josephson current originates from first-order tunneling processes. Consequently, an s-wave component of the superconducting order parameter has to be present also in BSCCO. In a strict sense, the data show the existence of the s component only in the vicinity of the interface and at temperatures below the T_c of Pb. However, the temperature dependence of the critical current strongly indicates that the T_c of the s component is well above the T_c of Pb, and therefore it seems unlikely that the s component of BSCCO is simply induced by the proximity of Pb. The low values of the measured I_cR_N products and the temperature dependence of the critical current show that the fraction Δ_s/Δ_d is small, most likely below 10^{-3}. However, even

such a small *s* component is nontrivial since it cannot be explained simply by orthorhombicity or the presence of CuO chains as in YBCO. Most of our experiments have been performed on highly underdoped BSCCO making the situation even more interesting since possible *s*-wave contributions might rather be expected on the overdoped than on the underdoped side.

ACKNOWLEDGMENTS

The authors would like to thank G. Hechtfischer, A. S. Katz, R. A. Klemm, K. Schlenga, S. Schmitt, P. Müller, and O. Waldmann for valuable discussions. Financial support by the Bayerische Forschungsstiftung and the Deutsche Forschungsgemeinschaft is gratefully acknowledged.

[1] D. Pines, Physica B **199**, 330 (1994).
[2] D. J. Scalapino, Phys. Rep. **250**, 329 (1995).
[3] K. A. Müller, Nature (London) **377**, 133 (1995).
[4] R. A. Klemm, Phys. Rev. Lett. **73**, 1871 (1994).
[5] R. A. Klemm, Phys. Rev. B **55**, 3249 (1997).
[6] R. A. Klemm, C. T. Rieck, and K. Scharnberg, Phys. Rev. B **58**, 1051 (1998).
[7] R. B. Laughlin, Phys. Rev. Lett. **80**, 5188 (1998).
[8] D. A. Wollman, D. J. Van Harlingen, W. C. Lee, D. M. Ginsberg, and A. J. Leggett, Phys. Rev. Lett. **71**, 2134 (1993).
[9] Y. Kitaoka, J. Phys. Soc. Jpn. **62**, 2803 (1993).
[10] W. N. Hardy, D. A. Bonn, D. C. Morgan, R. Liang, and K. Zhang, Phys. Rev. Lett. **70**, 3999 (1993).
[11] D. A. Brawner and H. R. Ott, Phys. Rev. B **50**, 6530 (1994).
[12] C. C. Tsuei, J. R. Kirtley, C. C. Chi, Lock See Yu-Jahnes, A. Gupta, T. Shaw, J. Z. Sun, and M. B. Ketchen, Phys. Rev. Lett. **73**, 593 (1994).
[13] T. P. Devereaux, D. Einzel, B. Stadlober, R. Hackl, D. H. Leach, and J. J. Neumeier, Phys. Rev. Lett. **72**, 396 (1994); **72**, 3291 (1994).
[14] D. A. Wollman, D. J. van Harlingen, J. Giapintzakis, and D. M. Ginsberg, Phys. Rev. Lett. **74**, 797 (1995).
[15] J. R. Kirtley, C. C. Tsuei, J. Z. Sun, C. C. Chi, Lock Se Yu-Jahnes, A. Gupta, M. Rupp, and M. B. Ketchen, Nature (London) **373**, 225 (1995).
[16] A. Mathai, Y. Gim, R. C. Black, A. Amar, and F. C. Wellstood, Phys. Rev. Lett. **74**, 4523 (1995).
[17] J. H. Miller, Q. Y. Ying, Z. G. Zou, N. Q. Fan, J. H. Xu, M. F. Davis, and J. C. Wolfe, Phys. Rev. Lett. **74**, 2347 (1995).
[18] D. J. Van Harlingen, Rev. Mod. Phys. **67**, 515 (1995).
[19] D. A. Bonn, S. Kamal, A. Bonakdarpour, R. Liang, W. N. Hardy, C. C. Homes, D. N. Basov, and T. Timusk, Czech. J. Phys. **46**, 3195 (1996).
[20] H. Hilgenkamp, J. Mannhart, and B. Mayer, Phys. Rev. B **53**, 14 586 (1996).
[21] J. Mannhart, H. Hilgenkamp, B. Mayer, Ch. Gerber, J. R. Kirtley, K. A. Moler, and M. Sigrist, Phys. Rev. Lett. **77**, 2782 (1996).
[22] Y. Gim, A. Mathai, R. C. Black, A. Amar, and F. C. Wellstood, J. Phys. I **6**, 2299 (1996).
[23] D. A. Brawner and H. R. Ott, Phys. Rev. B **53**, 8249 (1996).
[24] M. Covington, R. Scheuerer, K. Bloom, and L. H. Greene, Appl. Phys. Lett. **68**, 1717 (1996).
[25] M. Covington, M. Aprili, E. E. Paraoanu, L. H. Greene, F. Xu, J. Zhu, and C. A. Mirkin, Phys. Rev. Lett. **79**, 277 (1997).
[26] L. Alff, H. Takashima, S. Kashiwaya, N. Terada, H. Ihara, Y. Tanaka, M. Koyanagi, and K. Kajimura, Phys. Rev. B **55**, R14 757 (1997).
[27] H. Walter, W. Prusseit, R. Semerad, H. Kinder, W. Assmann, H. Huber, H. Burkhardt, D. Rainer, and J. A. Sauls, Phys. Rev. Lett. **80**, 3598 (1998).
[28] Z. X. Shen, D. S. Dessau, B. O. Wells, D. M. King, W. E. Spicer, A. J. Arko, D. Marshall, L. W. Lombardo, A. Kapitulnik, P. Dickinson, S. Doniach, J. diCarlo, A. G. Loesser, and G. H. Park, Phys. Rev. Lett. **70**, 1553 (1993).
[29] H. Ding, T. Yokoya, J. C. Campuzano, T. Takahashi, M. Randeria, M. R. Norman, T. Mochiku, K. Kadowaki, and J. Giapintzakis, Nature (London) **382**, 51 (1996).
[30] O. Waldmann, F. Steinmeyer, P. Müller, J. J. Neumeier, F. X. Regi, H. Savary, and J. Schneck, Phys. Rev. B **53**, 11 825 (1996).
[31] J. R. Kirtley, C. C. Tsuei, M. Rupp, J. Z. Sun, Lock-See Yu-Jahnes, A. Gupta, M. B. Ketchen, K. A. Moler, and M. Bhushan, Phys. Rev. Lett. **76**, 1336 (1996).
[32] J. R. Kirtley, C. C. Tsuei, K. A. Moler, J. Z. Sun, A. Gupta, Z. F. Ren, J. H. Wang, Z. Z. Li, H. Raffy, J. Mannhart, H. Hilgenkamp, B. Mayer, and Ch. Gerber, Czech. J. Phys. **46**, 3168 (1996).
[33] J. R. Kirtley, C. C. Tsuei, H. Raffy, Z. Z. Li, A. Gupta, J. Z. Sun, and S. Megtert, Europhys. Lett. **36**, 707 (1996).
[34] C. C. Tsuei and J. R. Kirtley, Physica C **282**, 4 (1997).
[35] C. C. Tsuei, J. R. Kirtley, M. Rupp, J. Z. Sun, A. Gupta, M. B. Ketchen, C. A. Wang, Z. F. Ren, J. H. Wang, and M. Bhushan, Science **271**, 329 (1996).
[36] L. Ozyuzer, Z. Yusof, J. F. Zasadzinski, R. Mogilevsky, D. G. Hinks, and K. E. Gray, Phys. Rev. B **57**, R3245 (1998).
[37] A. G. Sun, D. A. Gajewski, M. B. Maple, and R. C. Dynes, Phys. Rev. Lett. **72**, 2267 (1994).
[38] A. G. Sun, L. M. Paulius, D. A. Gajewski, M. B. Maple, and R. C. Dynes, Phys. Rev. B **50**, 3266 (1994).
[39] R. C. Dynes, Solid State Commun. **92**, 62 (1994).
[40] A. S. Katz, A. G. Sun, R. C. Dynes, and K. Char, Appl. Phys. Lett. **66**, 105 (1995).
[41] A. G. Sun, S. H. Han, A. S. Katz, D. A. Gajewski, M. B. Maple, and R. C. Dynes, Phys. Rev. B **52**, R15 731 (1995).
[42] A. G. Sun, A. Truscott, A. S. Katz, R. C. Dynes, B. W. Veal, and C. Gu, Phys. Rev. B **54**, 6734 (1996).
[43] R. Kleiner, A. S. Katz, A. G. Sun, R. Summer, D. A. Gajewski, S. H. Han, S. I. Woods, E. Dantsker, B. Chen, K. Char, M. B. Maple, R. C. Dynes, and John Clarke, Phys. Rev. Lett. **76**, 2161 (1996).
[44] J. Lesueur, M. Aprili, A. Goulon, T. J. Horton, and L. Dumoulin, Phys. Rev. B **55**, R3398 (1997).
[45] K. A. Kouznetsov, A. G. Sun, B. Chen, A. S. Katz, S. R. Bahcall, J. Clarke, R. C. Dynes, D. A. Gajewski, S. H. Han, M. B. Maple, J. Giapintzakis, J.-T. Kim, and D. M. Ginsberg, Phys. Rev. Lett. **79**, 3050 (1997).
[46] M. Willemin, C. Rossel, J. Hofer, H. Keller, Z. F. Ren, and J. H. Wang, Phys. Rev. B **57**, 6137 (1998).
[47] Q. Li, Y. N. Tsay, M. Suenaga, G. D. Gu, and N. Koshizuga, Physica C **282**, 1495 (1997).

[48] Q. Li, Y. N. Tsay, Y. Thu, M. Suenaga, G. D. Gu, and N. Koshizuga, IEEE Trans. Appl. Supercond. **7**, 1584 (1997).
[49] P. Coppens, P. Lee, Y. Gao, and H.-S. Sheu, J. Phys. Chem. Solids **52**, 1267 (1991).
[50] M. Cardona, T. Strohm, and X. Zhou, Physica C **282-287**, 222 (1997); T. Strohm and M. Cardona, Phys. Rev. B **55**, 12 725 (1997); Solid State Commun. **104**, 223 (1997).
[51] R. A. Klemm, C. T. Rieck, and K. Scharnberg (unpublishd).
[52] H. Z. Durusoy, D. Lew, L. Lombardo, A. Kapitulnik, T. H. Geballe, and M. R. Beasley, Physica C **266**, 253 (1996).
[53] S. Sinha and K.-W. Ng, Phys. Rev. Lett. **80**, 1296 (1998).
[54] R. Kleiner, M. Mößle, W. Walkenhorst, G. Hechtfischer, K. Schlenga, and P. Müller, Physica C **282**, 2435 (1997).
[55] J. M. Rowell, in *Tunneling Phenomena in Solids*, edited by E. Burstein and S. Lundquist (Plenum, New York, 1969).
[56] Y. Tanaka, Phys. Rev. Lett. **72**, 3871 (1994).
[57] R. Kleiner, F. Steinmeyer, G. Kunkel, and P. Müller, Phys. Rev. Lett. **68**, 2394 (1992).
[58] R. Kleiner and P. Müller, Phys. Rev. B **49**, 1327 (1994).
[59] J. U. Lee, J. E. Nordman, and G. Hohenwarter, Appl. Phys. Lett. **67**, 1471 (1995); J. U. Lee, P. Guptasarma, D. Hornbaker, A. El-Kortas, D. Hinks, and K. E. Gray, *ibid.* **71**, 1412 (1997).
[60] A. Yurgens, D. Winkler, N. V. Zavaritzky, and T. Claeson, Phys. Rev. B **53**, 8887 (1996).
[61] A. Yurgens, D. Winkler, N. V. Zavaritsky, and T. Claeson, Phys. Rev. Lett. **79**, 5122 (1997).
[62] Yu. I. Latyshev, J. E. Nevelskaya, and P. Monceau, Phys. Rev. Lett. **77**, 932 (1996).
[63] Y. G. Xiao, R. Dömel, C. L. Jia, C. Osterhöver, and H. Kohlstedt, Supercond. Sci. Technol. **9**, A22 (1996).
[64] P. Seidel, A. Pfuch, U. Hübner, F. Schmidl, H. Schneidewind, T. Ecke, and J. Scherbel, Physica C **293**, 49 (1997).
[65] J. Takeya, S. Akita, J. Shimoyama, and K. Kishio, Physica C **261**, 21 (1996).
[66] T. Yasuda, M. Tonouchi, and S. Takano, Czech. J. Phys. **46**, 1265 (1996).
[67] K. Tanabe, Y. Hidaka, S. Karimoto, and M. Suzuki, Phys. Rev. B **53**, 9348 (1996).
[68] M. Itoh, S. Karimoto, K. Mamekawa, and M. Suzuki, Phys. Rev. B **55**, 12 001 (1997).
[69] M. Sakai, A. Odagawa, H. Adachi and K. Setsune, Physica C **293**, 55 (1997)
[70] R. Kleiner and P. Müller, Physica C **293**, 156 (1997).
[71] W. Gerhäuser, H.-W. Neumüller, W. Schmidt, G. Ries, G. Saemann-Ischenko, H. Gerstenberg, and F.-M. Sauerzopf, Physica C **185**, 2273 (1991).
[72] D.E. McCumber, J. Appl. Phys. **39**, 3113 (1968).
[73] W.C. Stewart, Appl. Phys. Lett. **12**, 277 (1968).
[74] A. Barone and G. Paterno, *Physics and Applications of the Josephson Effect* (Wiley, New York, 1982).
[75] P.W. Anderson, *Lectures on the Many-Body Problem* (Academic Press, New York, 1964), Vol. 2.
[76] Ch. Renner and Ø. Fischer, Phys. Rev. B **51**, 9208 (1995).
[77] K. Schlenga, R. Kleiner, G. Hechtfischer, M. Mößle, S. Schmitt, P. Müller, Ch. Helm, Ch. Preis, F. Forsthofer, J. Keller, H. L. Johnson, M. Veith, and E. Steinbeiß, Phys. Rev. B **57**, 14 518 (1998).
[78] Y. Tanaka and S. Kashiwaya, Phys. Rev. B **56**, 892 (1997).
[79] R. Klemm (private communication).
[80] B. Mühlschlegel, Z. Phys. **155**, 313 (1959).
[81] N. Miyakawa, P. Guptasarma, J. F. Zasadzinski, D. G. Hinks, and K. E. Gray, Phys. Rev. Lett. **80**, 157 (1998).
[82] M. D. Fiske, Rev. Mod. Phys. **36**, 221 (1964).